Unified treatment of quantum coherent and incoherent hopping dynamics in electronic energy transfer: Reduced hierarchy equation approach

Akihito Ishizaki and Graham R. Fleming

Citation: The Journal of Chemical Physics **130**, 234111 (2009); doi: 10.1063/1.3155372
View online: http://dx.doi.org/10.1063/1.3155372
View Table of Contents: http://scitation.aip.org/content/aip/journal/jcp/130/23?ver=pdfcov
Published by the AIP Publishing

Unified treatment of quantum coherent and incoherent hopping dynamics in electronic energy transfer: Reduced hierarchy equation approach

Akihito Ishizaki and Graham R. Fleming[a)]
Department of Chemistry, University of California, Berkeley, California 94720, USA and Physical Bioscience Division, Lawrence Berkeley National Laboratory, Berkeley, California 94720, USA

(Received 12 December 2008; accepted 11 May 2009; published online 18 June 2009)

A new quantum dynamic equation for excitation energy transfer is developed which can describe quantum coherent wavelike motion and incoherent hopping in a unified manner. The developed equation reduces to the conventional Redfield theory and Förster theory in their respective limits of validity. In the regime of coherent wavelike motion, the equation predicts several times longer lifetime of electronic coherence between chromophores than does the conventional Redfield equation. Furthermore, we show quantum coherent motion can be observed even when reorganization energy is large in comparison to intersite electronic coupling (the Förster incoherent regime). In the region of small reorganization energy, slow fluctuation sustains longer-lived coherent oscillation, whereas the Markov approximation in the Redfield framework causes infinitely fast fluctuation and then collapses the quantum coherence. In the region of large reorganization energy, sluggish dissipation of reorganization energy increases the time electronic excitation stays above an energy barrier separating chromophores and thus prolongs delocalization over the chromophores.
 [DOI: 10.1063/1.3155372]

I. INTRODUCTION

Quantum dynamic phenomena are ubiquitous in molecular processes, and yet remain a challenge for experimental and theoretical investigations. On the experimental side, it has become possible to explore molecules on a time scale down to a few femtoseconds. This progress in ultrafast spectroscopy has opened up real-time observation of dynamic processes in complex chemical and biological systems, and has provided a strong impetus to theoretical studies of condensed phase quantum dynamics.

Recently, techniques of two-dimensional Fourier transform electronic spectroscopy[1–3] have been applied to explore photosynthetic light harvesting complexes. Engel *et al.*[4] investigated photosynthetic excitation energy transfer (EET) in the Fenna–Matthews–Olson (FMO) protein[5,6] of green sulfur bacteria. This protein is a trimer made of identical subunits, each of which contains seven bacteriochlorophyll (BChl) molecules, and is tasked with transporting sunlight energy collected in the chlorosome antenna to the reaction center, where charge separation is initiated. Their experiment revealed the existence of long-lived quantum coherence between electronic excited states of BChls in the FMO protein. The observed coherence clearly lasts for time scales similar to the EET time scales, implying that electronic excitations move coherently through the FMO protein rather than by incoherent hopping motion as has usually been assumed.[7,8] Furthermore, Lee *et al.*[9] revealed coherent dynamics in the reaction center of purple bacteria by applying a two-color electronic coherence photon echo technique. The two spectroscopic observations raise obvious questions regarding the role of the protein environment in protecting the quantum coherence, and the significance of quantum superposition states in generating an efficiency of near unity in the quantum yield of photosynthetic EET. In order to address these questions, detailed theoretical investigations and novel theoretical frameworks are required in addition to further experimental studies.[10–14]

One of the viable approaches to explore long-lived quantum coherence and its interplay with the protein environment in EET processes is the reduced equation of motion. In this approach, the key quantity of interest is the reduced density matrix, i.e., the partial trace of the total density matrix over the environmental degrees of freedom. The most commonly used theory from this approach is the Redfield equation,[15–18] which is based on second-order perturbative truncation with respect to electron-environment interaction and the Markov approximation. In photosynthetic EET, each site of a multichromophoric array is coupled to its local environmental phonons. Additionally, electronic de-excitation of a donor chromophore and excitation of an acceptor occur via nonequilibrium phonon states in accordance with the vertical Franck–Condon transition. The phonons coupled to each chromophore then relax to their respective equilibrium states on a characteristic time scale. This process becomes more significant when the reorganization energies are not small in comparison to the electronic coupling—a typical situation in photosynthetic EET. In the FMO protein, for example, the electronic coupling strengths span a wide range, $1-100\ \mathrm{cm}^{-1}$, while the suggested reorganization energies span a similar range.[3,19,20] However, these site-dependent reorganization processes cannot be described by the Redfield equation due to the Markov approximation. The Markov approximation requires the phonons to relax to their equilib-

[a)]Electronic mail: grfleming@lbl.gov.

rium states instantaneously, that is, the phonons are always in equilibrium even under the electron-phonon interaction.[21]

In order to go beyond the Markov approximation, a feasible path is to employ non-Markovian quantum master equations such as the Nakajima–Zwanzig equation[22,23] (time-convolution formalism) or the Shibata–Takahashi–Hashitsume equation[24] (time-convolutionless formalism) based on projection operator techniques. They are mathematically exact and hold for arbitrary systems and interactions; however, it is impossible to reduce explicit expressions for the equations beyond the exact formal structures. Hence, the second-order perturbative expansion with respect to system-environmental interaction is usually invoked to make practical calculations possible. Under the second-order perturbation theory, however, the time-convolution equation of the Nakajima–Zwanzig type can be proven to correspond to the two-state-jump model.[25,26] The optical line shapes calculated by the equation contain unphysical peak splitting in strong non-Markovian regime entailing sluggish fluctuations and/or dissipation of large reorganization energy. Hence, the equation is applicable only for the nearly Markovian regime. On the other hand, the time-convolutionless equation of the Shibata–Takahashi–Hashitsume type can be recast into the well-known time-dependent Redfield equation in the eigenstate representation,

$$\frac{\partial}{\partial t}\rho_{\mu\nu}(t) = -i\omega_{\mu\nu}\rho_{\mu\nu}(t) + \sum_{\mu'\nu'} R_{\mu\nu,\mu'\nu'}(t)\rho_{\mu'\nu'}(t), \quad (1.1)$$

where $\omega_{\mu\nu}$ is the energy gap between the μth and νth eigenstates and the time-dependent relaxation tensors, $R_{\mu\nu,\mu'\nu'}(t)$, are responsible for non-Markovian nature. This equation has a mathematical advantage of time locality without involving any integrodifferential form. Due to this time locality, however, the phonon modes associated with each chromophore can relax *independently* of electronic states of the chromophores. For this reason, the equation cannot capture the above mentioned site-dependent reorganization processes in spite of its non-Markovian nature. In addition, after the correlation time of phonon-induced fluctuations, the time-dependent relaxation tensors converge to steady values, $R_{\mu\nu,\mu'\nu'}(t=\infty)$, that is, the EET after the correlation time is described by the Markovian Redfield equation.

In order to elucidate the origin of the long-lived quantum coherence and its interplay with the protein environment in EET processes, it is crucial to consider and describe the dynamics of environmental phonons in a more detailed fashion. In this work, we tackle the development of a new theoretical framework which can describe the above mentioned site-dependent reorganization dynamics of environmental phonons. For this purpose, we utilize the Gaussian property of phonon operators in the electron-phonon interaction Hamiltonian. A remark which should be made here is that the cumulant expansion up to second order is rigorous for phonon operators owing to the Gaussian property, whereas the second-order perturbative truncation is just an approximation. Further we employ the overdamped Brownian oscillator model[27] and the hierarchical expansion technique[25,28–30] to obtain a practical expression for the reduced equation of motion. The developed equation can describe quantum coherent wavelike motion and incoherent hopping in the same framework, and reduces to the conventional Redfield theory and Förster theory in their respective limits of validity. Furthermore, the equation predicts several times longer-lived quantum coherence between electronic excited states of chromophores than the conventional Redfield equation does. The paper is organized as follows: In Sec. II, we describe new formalism of quantum dynamics in excitation energy transfer. In Sec. III, we present and discuss numerical results for the formalism developed in Sec. II Finally, Sec. IV is devoted to concluding remarks.

II. FORMULATION

In this paper, we discuss the simplest electronic energy transfer system, a dimer (a spin-boson-type model[31]). We employ the following Frenkel exciton Hamiltonian to study excitation energy transfer dynamics,[32]

$$H_{\mathrm{tot}} \equiv H^{\mathrm{el}} + H^{\mathrm{ph}} + H^{\mathrm{reorg}} + H^{\text{el-ph}}, \quad (2.1)$$

where

$$H^{\mathrm{el}} = \sum_{j=1}^{2} |j\rangle \varepsilon_j^0 \langle j| + J_{12}(|1\rangle\langle 2| + |2\rangle\langle 1|), \quad (2.2a)$$

$$H^{\mathrm{ph}} = \sum_{j=1}^{2} H_j^{\mathrm{ph}}, \quad (2.2b)$$

$$H^{\mathrm{reorg}} = \sum_{j=1}^{2} |j\rangle \lambda_j \langle j|, \quad (2.2c)$$

and

$$H^{\text{el-ph}} = \sum_{j=1}^{2} H_j^{\text{el-ph}} = \sum_{j=1}^{2} V_j u_j. \quad (2.2d)$$

In the above, $|j\rangle$ represents the state where only the jth site is in its excited electronic state $|\varphi_{je}\rangle$ and another is in its ground electronic state $|\varphi_{kg}\rangle$, i.e., $|j\rangle \equiv |\varphi_{je}\rangle|\varphi_{kg}\rangle$. In addition, we define the ground state $|0\rangle$ as $|0\rangle \equiv |\varphi_{1g}\rangle|\varphi_{2g}\rangle$. Equation (2.2a) is the electronic Hamiltonian in which the Hamiltonian of the ground electronic state is set to be zero by definition. ε_j^0 is the excited electronic energy of the jth site in the absence of phonons. J_{12} is the electronic coupling between the two sites, which responsible for EET between the individual sites. In Eq. (2.2b), $H_j^{\mathrm{ph}} \equiv \Sigma_\xi \hbar\omega_\xi (p_\xi^2 + q_\xi^2)/2$ is the phonon Hamiltonian associated with the jth site, where q_ξ, p_ξ, and ω_ξ are the dimensionless coordinate, conjugate momentum, and frequency of the ξth phonon mode, respectively. In Eq. (2.2c), $\lambda_j \equiv \Sigma_\xi \hbar\omega_\xi d_{j\xi}^2/2$ is the reorganization energy of the jth site, where $d_{j\xi}$ is the dimensionless displacement of the equilibrium configuration of the ξth phonon mode between the ground and excited electronic states of the jth site. In Eq. (2.2d), $H_j^{\text{el-ph}}$ is the coupling Hamiltonian between the jth site and the phonon modes and we have defined $u_j \equiv -\Sigma_\xi \hbar\omega_\xi d_{j\xi} q_\xi$ and $V_j \equiv |j\rangle\langle j|$. For simplicity we assume the phonon modes associated with one site are un-

correlated with those of another site. The Liouvillian for the Hamiltonian in Eq. (2.1) is decomposed as

$$\mathcal{L}^{\text{tot}} = \mathcal{L}_e + \mathcal{L}^{\text{ph}} + \mathcal{L}^{\text{el-ph}}, \tag{2.3}$$

where $\mathcal{L}_e$, $\mathcal{L}^{\text{ph}}$, and $\mathcal{L}^{\text{el-ph}}$ correspond to $H_e \equiv H^{\text{el}} + H^{\text{reorg}}$, H^{ph}, and $H^{\text{el-ph}}$, respectively.

Now, we identify the electronic excitations as the relevant system. The phonon degrees of freedom constitute the heat bath responsible for electronic energy fluctuations and dissipation of reorganization energy. An adequate description of the EET dynamics is given by the reduced density operator $\rho(t)$, that is, the partial trace of the total density operator $\rho^{\text{tot}}(t)$ over the irrelevant phonon degrees of freedom: $\rho(t) = \text{Tr}_{\text{ph}}\{\rho^{\text{tot}}(t)\}$. In order to reduce the total density operator, we suppose that the total system at the initial time $t=0$ is in the factorized product state of the form, $\rho^{\text{tot}}(0) \equiv \rho(0) \otimes \exp(-\beta H^{\text{ph}})/Z$, where $\beta \equiv 1/k_B T$ and $Z \equiv \text{Tr}_{\text{ph}} \exp(-\beta H^{\text{ph}})$. This factorized initial condition is generally unphysical since it neglects an inherent correlation between a system and its environment. Hence, it may lead to serious issues in the time evolution of the reduced density operator.[30,33–38] In electronic excitation processes, however, this initial condition is of no consequence because it corresponds to the electronic ground state or an electronic excited state generated by photoexcitation in accordance to the vertical Franck–Condon transition. The reduced density operator $\rho(t)$ evolves in time as follows:

$$\tilde{\rho}(t) = \tilde{\mathcal{U}}(t)\tilde{\rho}(0), \tag{2.4}$$

where the interaction picture has been employed and a tilde indicates an operator in the interaction picture: $\tilde{O}(t) \equiv e^{i\mathcal{L}_e t} O$ for any operator O. The reduced propagator $\tilde{\mathcal{U}}(t)$ is expressed as

$$\tilde{\mathcal{U}}(t) \equiv \langle T_+ \exp\left[-i\int_0^t ds \tilde{\mathcal{L}}^{\text{el-ph}}(s)\right]\rangle_{\text{ph}}, \tag{2.5}$$

where $\langle \ldots \rangle_{\text{ph}}$ stands for $\text{Tr}_{\text{ph}}\{\ldots \exp(-\beta H^{\text{ph}})\}/Z$ and the symbol T_+ describes the usual chronological time ordering of $\tilde{\mathcal{L}}^{\text{el-ph}}(t)$. Here, we notice that Wick's theorem[39] yields the Gaussian property for the phonon operator u_j as follows:

$$\langle \mathcal{T}\tilde{u}_j(t_{2n})\tilde{u}_j(t_{2n-1}) \ldots \tilde{u}_j(t_2)\tilde{u}_j(t_1)\rangle_{\text{ph}} = \sum_{\text{a.p.p.}} \prod_{k,\ell} \langle \mathcal{T}\tilde{u}_j(t_k)\tilde{u}_j(t_\ell)\rangle_{\text{ph}}, \tag{2.6}$$

where the sum is over all possible ways of picking pairs (a.p.p) among $2n$ operators, and the symbol $\mathcal{T}$ denotes an ordering operator which orders products by some rule, e.g., the chronological time ordering operator $\mathcal{T}=T_+$. Therefore, Eq. (2.5) can be recast into

$$\tilde{\mathcal{U}}(t) = T_+ \prod_{j=1}^{2} \exp\left[\int_0^t ds \tilde{W}_j(s)\right], \tag{2.7}$$

with

$$\tilde{W}_j(t) = -\frac{1}{\hbar^2}\int_0^t ds \tilde{V}_j(t)^{\times} \times \left[S_j(t-s)\tilde{V}_j(s)^{\times} - i\frac{\hbar}{2}\chi_j(t-s)\tilde{V}_j(s)^{\circ}\right], \tag{2.8}$$

where we have introduced the hyperoperator notations, $O^{\times} f \equiv [O,f]$ (a commutator) and $O^{\circ} f \equiv \{O,f\}$ (an anticommutator), for any operator O and operand operator f. Equation (2.7) is the cumulant expansion of Eq. (2.5) up to second order. In Eq. (2.8), $S_j(t)$ is the symmetrized correlation function of $\tilde{u}_j(t)$ expressed as

$$S_j(t) = \tfrac{1}{2}\langle\{\tilde{u}_j(t),\tilde{u}_j(0)\}\rangle_{\text{ph}}, \tag{2.9}$$

which describe fluctuations of the electronic energy of the jth site. On the other hand, $\chi_j(t)$ is the response function defined by

$$\chi_j(t) = \frac{i}{\hbar}\langle[\tilde{u}_j(t),\tilde{u}_j(0)]\rangle_{\text{ph}}, \tag{2.10}$$

which describes the dissipation of the phonon reorganization energy associated with the jth site.[40] From Eqs. (2.4) and (2.7), we obtain the equation of motion for the reduced density operator $\rho(t)$ as follows:

$$\frac{\partial}{\partial t}\tilde{\rho}(t) = T_+ \sum_{j=1}^{2} \tilde{W}_j(t)\tilde{\rho}(t). \tag{2.11}$$

Note that Eq. (2.11) is not a time-local equation unlike the time-dependent Redfield equation, Eq. (1.1), owing to the chronological time ordering operator T_+, which resequences and mixes the hyperoperators $\tilde{V}^{\times}(t)$ and $\tilde{V}^{\circ}(t)$ comprised in $\tilde{W}_j(t)$ and $\tilde{\rho}(t)$.

Here, we consider two limiting cases of Eq. (2.11). First, if the Markov approximation is employed, Eq. (2.11) reduces to the well-known second-order perturbative quantum master equation,[18]

$$\frac{\partial}{\partial t}\rho(t) = -i\mathcal{L}_e\rho(t) - \sum_{j=1}^{2} V_j^{\times}[\Lambda_j\rho(t) - \rho(t)\Lambda_j^{\dagger}], \tag{2.12a}$$

with

$$\Lambda_j \equiv \frac{1}{\hbar^2}\int_0^{\infty} dt C_{jj}(t) e^{-iH_e t/\hbar} V_j e^{iH_e t/\hbar}, \tag{2.12b}$$

where we have introduced the phonon correlation function, $C_{jj}(t) \equiv \langle \tilde{u}_j(t)\tilde{u}_j(0)\rangle_{\text{ph}}$. Equation (2.12) is transformed to the full Redfield equation in the eigenstate representation, $H_e|e_\mu\rangle = E_\mu|e_\mu\rangle$, where E_μ and $|e_\mu\rangle$ are the μth eigenenergy and the corresponding eigenstate, respectively. In the representation, the matrix element of Eq. (2.12b) can be expressed as

$$\langle e_\mu|\Lambda_j|e_\nu\rangle = \frac{1}{\hbar^2}\langle e_\mu|V_j|e_\nu\rangle C_{jj}[\omega_{\nu\mu}], \tag{2.13}$$

where $C_{jj}[\omega] \equiv \int_0^{\infty} dt e^{i\omega t} C_{jj}(t)$ and $\omega_{\nu\mu} \equiv (E_\nu - E_\mu)/\hbar$. According to Eq. (2.13), in order to get a nonvanishing transition rate between two eigenstates, the energy gap between them must be matched with the frequency of a phonon mode. Con-

sequently a transition through hot phonon states or a multiphonon transition cannot be captured in the Redfield framework, as examined by Yang and Fleming.[32] This shortcoming is an artifact caused by the second-order perturbative expression, Eq. (2.12), as the consequence of the Markov approximation. However, Eq. (2.11) itself is a non-Markovian equation derived in a nonperturbative manner with respect to the electron-phonon coupling, and thus Eq. (2.11) can describe multiphonon transition processes, which play a role in Förster-type incoherent hopping EET.[32] In the second place, when the intersite electronic coupling J_{12} is vanishingly small, we have $\tilde{V}_j(t) \simeq V_j = |j\rangle\langle j|$ in Eq. (2.8). In this limit, Eq. (2.11) leads to

$$\langle j|\rho(t)|0\rangle = e^{-i(\varepsilon_j^0+\lambda_j)t/\hbar - g_j(t)}\langle j|\rho(0)|0\rangle, \tag{2.14}$$

where $g_j(t)$ is the line shape function[27] defined by $g_j(t) \equiv \int_0^t ds \int_0^s ds' C_{jj}(s')/\hbar^2$. The Fourier transform of Eq. (2.14) yields the absorption spectrum of the jth site, which plays an important role in Förster theory.[41,42] According to Förster theory an incoherent hopping rate from the jth site to the kth site is given by[32]

$$k_{k\leftarrow j}^F = \frac{J_{jk}^2}{\hbar^2}\int_{-\infty}^{\infty}\frac{d\omega}{2\pi}A_k[\omega]F_j[\omega], \tag{2.15}$$

where $A_j[\omega]$ and $F_j[\omega]$ are the absorption and fluorescence spectra of the jth site, respectively, and are expressed as

$$A_j[\omega] = \int_0^{\infty} dt e^{i\omega t} e^{-i(\varepsilon_j^0+\lambda_j)t/\hbar - g_j(t)}, \tag{2.16a}$$

$$F_j[\omega] = \int_0^{\infty} dt e^{i\omega t} e^{-i(\varepsilon_j^0-\lambda_j)t/\hbar - g_j^*(t)}. \tag{2.16b}$$

Since we have adopted the equilibrium phonon states associated with the electronic ground state as the initial condition, Eq. (2.11) cannot be reduced to the fluorescence spectrum directly. However, it is possible to obtain the fluorescence spectrum by integrating Eq. (2.11) numerically until the phonon states associated with the electronic excited state reach their equilibrium states, as will be discussed below.

The quantum fluctuation-dissipation relation[43] allows us to express the symmetrized correlation function and the response function as

$$S_j(t) = \frac{\hbar}{\pi}\int_0^{\infty} d\omega \chi_j''[\omega]\coth\frac{\beta\hbar\omega}{2}\cos\omega t, \tag{2.17}$$

$$\chi_j(t) = \frac{2}{\pi}\int_0^{\infty} d\omega \chi_j''[\omega]\sin\omega t, \tag{2.18}$$

where $\chi_j''[\omega]$ is termed the spectral distribution function defined by the imaginary part of the Fourier–Laplace transform of the response function: $\chi_j[\omega] = \int_0^{\infty} d\omega e^{i\omega t}\chi_j(t)$. The absolute magnitude of the spectral distribution function is related to the reorganization energy by $\lambda_j = \int_0^{\infty} d\omega \chi_j''[\omega]/(\pi\omega)$. Several forms of $\chi_j''[\omega]$ are employed in literature, either based on model assumptions or analyses of molecular simulations. In this paper, we employ the Drude–Lorentz density (the overdamped Brownian oscillator model):[30,27]

$$\chi_j''[\omega] = 2\lambda_j\frac{\omega\gamma_j}{\omega^2+\gamma_j^2}, \tag{2.19}$$

which has been successfully used for theoretical analyses of experimental results.[44–48] If we further assume the high-temperature condition characterized by $\beta\hbar\gamma_j < 1$, Eqs. (2.17) and (2.18) can be evaluated as

$$S_j(t) \simeq \frac{2\lambda_j}{\beta}e^{-\gamma_j t}, \quad \chi_j(t) = 2\lambda_j\gamma_j e^{-\gamma_j t}, \tag{2.20}$$

which satisfies the classical fluctuation-dissipation relation, $\chi_j(t) = -\beta(d/dt)S_j(t)$. The parameter γ_j characterizes a timescale of fluctuation of the electronic energy and dissipation of the phonon reorganization energy associated with the jth site. Typical values of γ_j for photosynthetic EET satisfy the high-temperature assumption. For example, we have $\beta\hbar\gamma_j = 0.25$ for a case of $\gamma_j^{-1} = 100$ fs and $T = 300$ K. If the high-temperature assumption cannot be applied, we can improve the formalism by employing the low-temperature correction in Ref. 49. Here, we should not overlook that the initial behaviors of the symmetrized correlation function $S_j(t)$ and the response function $\chi_j(t)$ are coarse grained. To be exact, the value of $\chi_j(0)$ should vanish by definition, and correspondingly the first time derivative of $S_j(t)$ at $t=0$ should also vanish. This coarse-grained nature is a drawback of the Drude–Lorentz density or the overdamped Brownian oscillator model, Eq. (2.19). However, as long as we discuss slow fluctuation and dissipation processes caused by the environmental phonons, this coarse-grained nature should not be a fatal defect. Substitution of Eq. (2.20) into Eq. (2.8) yields

$$\tilde{W}_j(t) = \int_0^t ds \tilde{\Phi}_j(t)e^{-\gamma_j(t-s)}\tilde{\Theta}_j(s), \tag{2.21}$$

where we have defined the phonon-induced relaxation operators as

$$\Phi_j \equiv iV_j^{\times}, \tag{2.22a}$$

$$\Theta_j \equiv i\left(\frac{2\lambda_j}{\beta\hbar^2}V_j^{\times} - i\frac{\lambda_j}{\hbar}\gamma_j V_j^{\circ}\right). \tag{2.22b}$$

Owing to the exponential function in Eq. (2.21), we can derive the following hierarchically coupled equations of motion for the reduced density operator $\rho(t)$:

$$\frac{\partial}{\partial t}\rho(t) = -i\mathcal{L}_e\rho(t) + \Phi_1\sigma^{(1,0)}(t) + \Phi_2\sigma^{(0,1)}(t), \tag{2.23a}$$

with

$$\frac{\partial}{\partial t}\sigma^{(n_1,n_2)}(t) = -(i\mathcal{L}_e + n_1\gamma_1 + n_2\gamma_2)\sigma^{(n_1,n_2)}(t) + \Phi_1\sigma^{(n_1+1,n_2)}(t) + n_1\Theta_1\sigma^{(n_1-1,n_2)}(t) + \Phi_2\sigma^{(n_1,n_2+1)}(t) + n_2\Theta_2\sigma^{(n_1,n_2-1)}(t), \tag{2.23b}$$

for non-negative integers (n_1,n_2). In Eq. (2.23), we have introduced operators defined by

$$\tilde{\sigma}^{(n_1,n_2)}(t) \equiv T_+\prod_{j=1}^{2}\left[\int_0^t ds e^{-\gamma_j(t-s)}\tilde{\Theta}_j(s)\right]^{n_j}\exp\left[\int_0^t ds\tilde{W}_j(s)\right]\tilde{\rho}(0). \tag{2.24}$$

When n_1 and n_2 are both equal to zero, Eq. (2.24) is reduced to

$$\tilde{\sigma}^{(0,0)}(t) = T_+\prod_{j=1}^{2}\exp\left[\int_0^t ds\tilde{W}_j(s)\right]\tilde{\rho}(0), \tag{2.25}$$

which is identical to the reduced density operator $\rho(t)$ expressed by Eqs. (2.4) and (2.7). The others $\{\sigma^{(n_1,n_2)}(t)\}$ are auxiliary operators to take into account fluctuation of the electronic energy and dissipation of reorganization energy. At the initial time $t=0$ just after the photoexcitation, all the auxiliary operators are set to be zero. It corresponds to a state where the phonon modes are in the equilibrium state in the absence of the electron-phonon coupling; however, it is a nonequilibrium state in the presence of such coupling. Hence, the coupling relaxes the phonons toward the actual equilibrium state, allowing the reorganization process to proceed. This reorganization dynamics is described as follows: After $t=0$, the matrix elements of $\{\sigma^{(n_1,n_2)}\}$ start to have nonzero values, and finally converge to the steady values. The steady states described by a full set of the hierarchical elements $(\rho,\{\sigma^{(n_1,n_2)}\})$ correspond to the actual equilibrium state in the presence of the electron-phonon coupling. In Fig. 1, we show the time evolution of a set of $(\rho,\{\sigma^{(n_1,n_2)}\})$. In order to clarify the role of the auxiliary elements $\{\sigma^{(n_1,n_2)}\}$, we calculated the time evolution only for site 1 in the absence of the intersite coupling, $J_{12}=0$, depicted in Fig. 1(a). For the calculation, we used the parameters, $\lambda_1=200\ \mathrm{cm}^{-1}$ and $\gamma_1=53\ \mathrm{cm}^{-1}(\gamma_1^{-1}=100\ \mathrm{fs})$. Figure 1(b) shows the time evolution of the populations of the reduced density operator $\langle 1|\rho(t)|1\rangle$ and the auxiliary operators $\{\langle 1|\sigma^{(n_1,n_2)}(t)|1\rangle\}$ where the phonons associated with site 2 is in equilibrium due to the absence of the interchromophoric coupling and then $n_2=0$. The red line indicates the evolution of $\langle 1|\rho(t)|1\rangle$, which is time independent because of no energy transfer. On the other hand, the blue lines represent the evolution of $\{\langle 1|\sigma^{(n_1,0)}(t)|1\rangle\}$. From top to bottom, the values of n_1 are 1, 2, 3, 4, and 5. We can recognize the elements $\{\sigma^{(n_1,0)}\}$ start to have nonzero values after $t=0$, and converge to the steady values on the time scale of $\gamma^{-1}=100$ fs. In order to confirm that the steady state corresponds to the equilibrium phonon state in the presence of the electron-phonon coupling, in Fig. 1(c), we calculated the emission spectrum from the electronic excited state $|\varphi_{1e}\rangle$ as a function of a delay time t after the photoexcitation. We normalized the intensity of Fig. 1(c) is such that the maximum value of the spectrum of $t=0$ is unity. The white line follows the maximum of the spectrum at a given delay time t. Just after the excitation, $t=0$, the maximum of the emission spectrum is located in the vicinity of $\omega=\varepsilon_1^0+\lambda_1$. The frequency of a maximum peak position lessens over time, and finally converges to the vicinity of

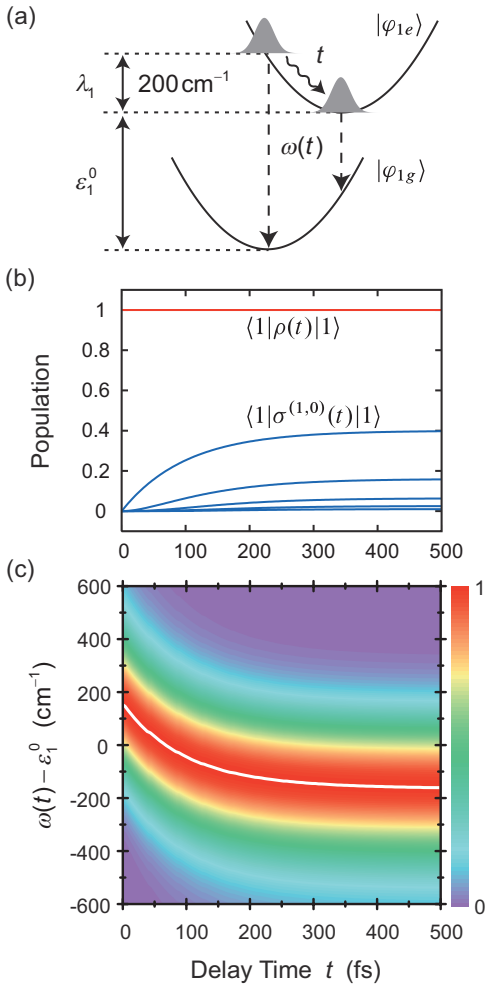

FIG. 1. (Color) Time evolution of phonon modes in the present formalism. In panel (a), the lower parabola is the electronic ground state of site 1 while the upper one is the electronic excited state. The gray packets illustrate the phonon states. The wavy arrow stands for the reorganization process. In panel (b), the red line presents the time evolution of the population of site 1. The blue lines show the time evolution of the matrix elements of the auxiliary operators, $\{\langle 1|\sigma^{(n_1,0)}|1\rangle\}$; from top to bottom, the values of n_1 are 1, 2, 3, 4, and 5. Panel (c) gives the emission spectrum calculated by the present theory, Eq. (2.23), as a function of a delay time t after photoexcitation. In panels (b) and (c), the parameters are set to be $\lambda_1=200\ \mathrm{cm}^{-1}$, $\gamma_1=53.08\ \mathrm{cm}^{-1}(\gamma^{-1}=100\ \mathrm{fs})$, and $T=150$ K. The normalization of the spectra is such that the maximum value is unity.

$\omega=\varepsilon_1^0-\lambda_1$. This phenomenon is the time-dependent Stokes shift.[40] As can be seen in Fig. 1(a), the emission spectrum with the convergent frequency, $\omega=\varepsilon_1^0-\lambda_1$, originates from the equilibrium phonons associated with the electronic excited state, and then the spectrum is identical to the fluorescence spectrum $F_1[\omega]$ in Eq. (2.16).

The hierarchically coupled equations Eq. (2.23b) continue to infinity, which is impossible to treat computationally. In order to terminate Eq. (2.23b) at a finite stage, we solve Eq. (2.23b) formally as

$$\sigma^{(n_1,n_2)}(t) = \int_0^t ds e^{-(i\mathcal{L}_e+n_1\gamma_1+n_2\gamma_2)(t-s)} \times[\Phi_1\sigma^{(n_1+1,n_2)}(s) + n_1\Theta_1\sigma^{(n_1-1,n_2)}(s) + \Phi_2\sigma^{(n_1,n_2+1)}(s) + n_2\Theta_2\sigma^{(n_1,n_2-1)}(s)]. \tag{2.26}$$

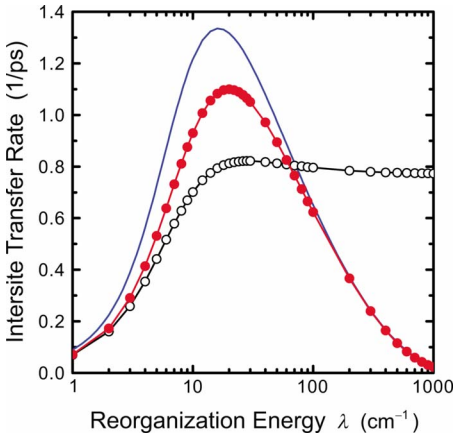

FIG. 2. (Color online) Intersite energy transfer rates from $|1\rangle$ to $|2\rangle$, $k_{2\leftarrow 1}$, as a function of reorganization energy, λ, predicted by the present theory, Eq. (2.23) (closed circles), the full-Redfield equation (open circles), and Förster theory (solid line). The other parameters are $\varepsilon_1^0-\varepsilon_2^0=100$ cm^{-1}, $J_{12}=20$ cm^{-1}, $\gamma=53$ cm^{-1}($\gamma^{-1}=100$ fs), and $T=300$ K. For theses parameters, the intersite dynamics is dominantly incoherent for the entire region depicted.

If $n_1\gamma_1+n_2\gamma_2$ is large enough compared to characteristic quantities for $\mathcal{L}_e$, ω_e, the kernel of the time integral can be replaced by Dirac's delta function as

$$(n_1\gamma_1+n_2\gamma_2)e^{-(n_1\gamma_1+n_2\gamma_2)(t-s)} \simeq \delta(t-s), \tag{2.27}$$

and hence Eq. (2.23b) can be approximated by

$$\frac{\partial}{\partial t}\sigma^{(n_1,n_2)}(t) = -i\mathcal{L}_e\sigma^{(n_1,n_2)}(t). \tag{2.28}$$

We replace Eq. (2.23b) by Eq. (2.28) for the integers, n_1 and n_2, satisfying

$$\mathcal{N} \equiv n_1+n_2 \gg \frac{\omega_e}{\min(\gamma_1,\gamma_2)}, \tag{2.29}$$

because this is a sufficient condition for $n_1\gamma_1+n_2\gamma_2 \gg \omega_e$. Since we can always choose a constant integer $\mathcal{N}$ to satisfy Eq. (2.29), the hierarchically coupled equations Eq. (2.23b) can be terminated at a finite stage.

III. DISCUSSION: NUMERICAL RESULTS

In this section, we present and discuss numerical results in order to examine the applicability of the present developed theory, Eq. (2.23). For simplicity, we assume that the phonon spectral distribution functions for the two sites are equivalent. Then, we have

$$\lambda_1=\lambda_2\equiv\lambda \quad \text{and} \quad \gamma_1=\gamma_2\equiv\gamma. \tag{3.1}$$

A. Weak electronic coupling

In this subsection, we consider a case with weak intersite coupling. In Fig. 2, we show the intersite energy transfer rates from site 1 to site 2, $k_{2\leftarrow 1}$, as a function of reorganization energy, λ, predicted by the present theory (closed circles). The other parameters are fixed to be $\varepsilon_1^0-\varepsilon_2^0=100$ cm^{-1}, $J_{12}=20$ cm^{-1}, $\gamma=53$ cm^{-1}($\gamma^{-1}=100$ fs), and $T=300$ K, which are typical for photosynthetic EET. The intersite dynamics calculated by using these parameters is dominantly incoherent for the entire region depicted in Fig. 2. In a region of small $\lambda(<5$ cm$^{-1})$, a weak coherent oscillation is observed at a short time; however, the oscillation does not affect the overall exponential-decay behavior. Therefore, we can assume the overall dynamics can be adequately analyzed by the following master equation:[50]

$$\frac{\partial}{\partial t}\langle 1|\rho|1\rangle = -k_{2\leftarrow 1}\langle 1|\rho|1\rangle + k_{1\leftarrow 2}\langle 2|\rho|2\rangle, \tag{3.2a}$$

$$\frac{\partial}{\partial t}\langle 2|\rho|2\rangle = +k_{2\leftarrow 1}\langle 1|\rho|1\rangle - k_{1\leftarrow 2}\langle 2|\rho|2\rangle. \tag{3.2b}$$

The transition rates $k_{2\leftarrow 1}$ and $k_{1\leftarrow 2}$ are determined as follows: For the initial condition $\langle 1|\rho(0)|1\rangle=1$, we calculate the time evolution of $\rho(t)$. We used the fourth-order Runge–Kutta method as the numerical propagation scheme. The time evolution of $\rho(t)$ does not strictly follow exponential decay kinetics because of the non-Markovian feature. Therefore, we determined the intersite transfer rates $k_{2\leftarrow 1}$ and $k_{1\leftarrow 2}$ with the least-square routine. For comparison, we show the rate calculated from the second-order quantum master equation, Eq. (2.12), or equivalently the Redfield equation in the full form[21] for the same parameters (open circles). Furthermore, as a benchmark for discussion of large reorganization energy cases, we also show the rate predicted by Förster theory, Eq. (2.15) (solid line).

In a region of small reorganization energy, the rate predicted by the present theory coincides with that of the full-Redfield equation. In this region, the relaxation of the reduced density matrix is much slower than the correlation time of the phonon-induced fluctuation, $\gamma^{-1}=100$ fs. This is the precondition which makes the Markov approximation appropriate for description of the quantum dynamics. In this case, the present theory reduces to the second-order quantum master equation, as mentioned in Eq. (2.12). The Markov approximation in the Redfield framework requires the phonon modes to relax to their equilibrium state instantaneously, that is, the phonons are always in equilibrium.[21] For the extremely small reorganization energy, the reorganization process does not play a major role; hence, the phonon modes are almost in equilibrium. As the result, we see the coincidence between the rates predicted by the present theory and the full-Redfield equation. However, such small reorganization energies are not likely to be physically realizable in molecular systems.

With increasing reorganization energy λ, the difference between the present theory and the full-Redfield equation becomes large. In a region of large reorganization energy, the rate predicted by the full-Redfield theory shows a λ-independent plateau.[21] However, the rate predicted by the present theory decreases with increasing λ, and is in accord with the Förster rate. In this region, the reorganization dynamics plays a major role. Electronic de-excitation of a donor chromophore and excitation of an acceptor occur via nonequilibrium phonon states in accordance with the Franck–Condon principle. The nonequilibrium states are dependent on the magnitude of reorganization energy. The phonons coupled to each chromophore then relax to their

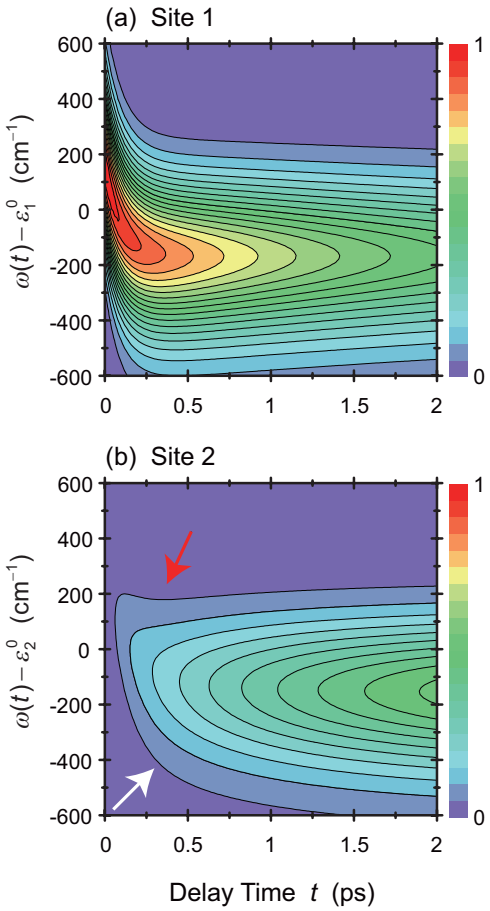

FIG. 3. (Color) Emission spectrum from site 1 (a) and site 2 (b) calculated by the present theory, Eq. (2.23), as a function of a delay time t after the photoexcitation of site 1. For the calculations, the parameters are chosen to be $\varepsilon_1^0-\varepsilon_2^0=100$ cm^{-1}, $J_{12}=20$ cm^{-1}, $\lambda=200$ cm^{-1}, $\gamma=53$ cm^{-1}($\gamma^{-1}=100$ fs), and $T=150$ K. The normalization of the spectra is such that the maximum value of panel (a) is unity. Twenty equally spaced contour levels from 0.05 to 1 are drawn.

respective equilibrium states. As noted in the companion paper,[21] this site-dependent reorganization dynamics cannot be described by the Redfield framework due to the Markov approximation. However, the present theory does describe the site-dependent reorganization dynamics. In order to demonstrate this, we present the dynamics of electronic excitation and the accompanying phonon modes as the emission spectra from site 1 and site 2 in Fig. 3. The reorganization energy is set to $\lambda=200$ cm^{-1}, and the temperature is changed to $T=150$ K in order to narrow the spectrum. The normalization of the spectra is such that the maximum value of the spectrum of site 1 is unity. Twenty equally spaced contour levels from 0.05 to 1 are drawn. Figure 3(a) is the emission spectrum from site 1 as a function of a delay time t after the photoexcitation of site 1. Just after the excitation, $t=0$, the maximum value of the emission spectrum is located in the vicinity of $\omega=\varepsilon_1^0+\lambda$. The frequency of a maximum peak position decreases with time, and reaches $\omega=\varepsilon_1^0-\lambda$ with almost constant magnitude. This indicates that the phonon reorganization dynamics takes place prior to the EET. This is reasonable because the interaction between the sites occurs at a rate of once every $J_{12}^{-1}=265$ fs($J_{12}=20$ cm^{-1}) whereas the time scale of the phonon reorganization process is $\gamma^{-1}=100$ fs. Figure 3(b) shows the emission spectrum from site 2. The contour line of the lowest level clearly shows that the emission spectrum emerges from close to $\omega=\varepsilon_2^0+\lambda$ in the short time region. This indicates that the excitation of site 2 occurs from the equilibrium phonons of the electronic ground state $|\varphi_{2g}\rangle$ to the nonequilibrium phonons of the electronic excited state $|\varphi_{2e}\rangle$ in accordance with the vertical Franck–Condon principle. Since the reorganization process takes place subsequently, we observe the emission spectrum in the vicinity of $\omega=\varepsilon_2^0-\lambda$ in the long time region. In contrast to the contour in the region indicated by the white arrow, the contour indicated by the red arrow is weakly dependent on the delay time t. This is because the excitation energy continuously flows into site 2 via the Franck–Condon state, and represents the above mentioned multiphonon transition process where the EET occurs through hot phonon states in the acceptor state. The observations from Fig. 3 can be summarized as follows: First, the reorganization process of the initial state, $|1\rangle=|\varphi_{1e}\rangle|\varphi_{2g}\rangle$, takes place. Subsequently, the electronic deexcitation of site 1 and the excitation of site 2 occurs from the equilibrium phonons of the initial state to the nonequilibrium phonons of the final state, $|2\rangle=|\varphi_{2e}\rangle|\varphi_{1g}\rangle$, in accordance to the Franck–Condon principle. Then, the reorganization process in the final state follows. It should be noticed that this sequential process is the assumption of Förster theory. For this reason, the rate predicted by the present theory agrees completely with the Förster rate in a region of large reorganization energy, $\lambda \gg J_{12}=20$ cm^{-1}, in Fig. 2.

In Fig. 2, the overall behavior of the rates predicted by the present theory and Förster theory are qualitatively similar. For incoherent EET, energy conservation is required between a donor state and an acceptor state. The energy conservation in the weak electronic coupling case is ensured by overlap of the donor fluorescence spectrum with the acceptor absorption spectrum. The spectra in the present theory and those in Förster theory are same. As the result, we observe qualitatively similar behavior between them. However, the Förster rate is derived on the basis of the assumption that intersite electronic coupling is very small compared to the reorganization energy. In regions of small or intermediate reorganization energy, $\lambda \lesssim J_{12}=20$ cm^{-1}, the perturbative assumption breaks down, and quantitative differences emerge.

B. Strong electronic coupling

In this subsection, we consider the quantum dynamics for the case of stronger electronic coupling. Figure 4 shows population dynamics of site 1 calculated by the present theory, Eq. (2.23), and the full-Redfield equation for various values of reorganization energy λ. As the initial condition for numerical calculation, we assume only site 1 is excited in accord to the Franck–Condon principle. The other parameters are fixed to be $\varepsilon_1^0-\varepsilon_2^0=100$ cm^{-1}, $J_{12}=100$ cm^{-1}, $\gamma=53.08$ cm^{-1}($\gamma^{-1}=100$ fs), and $T=300$ K. Figure 4(a) is for $\lambda=J_{12}/50=2$ cm^{-1}. The dynamics calculated by the two theories are almost coincident with each other. As mentioned in Sec. III A, the Markov approximation is appropriate in this case, because the relaxation of the reduced density matrix is much slower than the correlation time of the phonon-

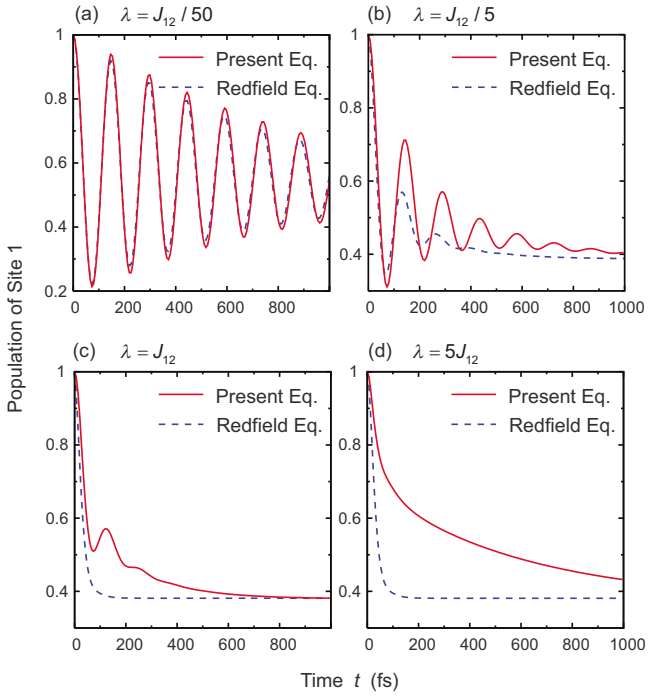

FIG. 4. (Color online) Time evolution of the population of site 1 calculated by the present theory, Eq. (2.23) (solid line) and the full-Redfield equation (dashed line) for various magnitudes of the reorganization energy λ. The other parameters are fixed to be $\varepsilon_1^0-\varepsilon_2^0=100$ cm^{-1}, $J_{12}=100$ cm^{-1}, $\gamma=53.08$ cm^{-1}($\gamma^{-1}=100$ fs), and $T=300$ K.

induced fluctuation, $\gamma^{-1}=100$ fs. However, increasing the reorganization energy produces a difference between the dynamics calculated by the two theories. Figure 4(b) shows the case of $\lambda=J_{12}/5=20$ cm^{-1}, which is still small compared to the electronic coupling and a regime of quantum coherent motion. The dynamics calculated by the present theory shows long-lasting coherent motion up to 1000 fs, which reflects the existence of long-lived quantum superposition between $|1\rangle$ and $|2\rangle$. On the other hand, the dynamics from the Redfield theory dephases on the timescale less than 400 fs. The cause of the difference is the breakdown of the Markov approximation. The infinitely fast dissipation of reorganization energy then corresponds to infinitely fast fluctuation according to the fluctuation-dissipation relation. The infinitely fast fluctuation with relatively large amplitude collapses the quantum superposition state. As the result, the coherent motion in the Redfield theory is destroyed rapidly compared with the present theory. Figure 4(c) is for the case of $\lambda=J_{12}=100$ cm^{-1}, which is comparable to the electronic coupling. They are reasonable values for photosynthetic systems. The dynamics calculated from the Redfield theory shows no oscillation; however, the present theory predict wavelike motion up to 300 fs. Figure 4(d) presents the case of $\lambda=5J_{12}=500$ cm^{-1}, which is large compared to the electronic coupling and should produce incoherent hopping. As expected, the dynamic behavior of the Redfield theory is similar to that in Fig. 4(c) because the full-Redfield theory predicts λ-independent dynamics for large reorganization energy due to the Markov approximation.[21] The dynamics calculated by the present theory also shows no wavelike motion. However, it should be noted that the dynamics involves

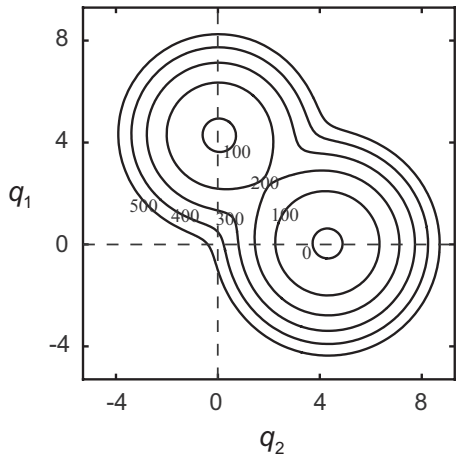

FIG. 5. Adiabatic potential surface $E^-(\mathbf{q})$ given by Eqs. (3.5). For the calculation, the parameters are chosen to be $\varepsilon_1^0=100$ cm^{-1}, $\varepsilon_2^0=0$ cm^{-1}, $J_{12}=100$ cm^{-1}, $\omega_\gamma=53.08$ cm^{-1}, and $\lambda_\gamma=500$ cm^{-1}($d_\gamma=4.34$). Six equally spaced contour levels from 0 to 500 are drawn. The local minimum located around $(q_1,q_2)=(4,0)$ corresponds to site 1, whereas that around $(q_1,q_2)=(0,4)$ is site 2. The point of origin corresponds to the Franck–Condon state.

two time scales. Comparing Fig. 4(d) with Figs. 4(a)–4(c), we can recognize that the faster component ($t\lesssim 100$ fs) arises from quantum coherence. The quantum coherent motion is destroyed before the first oscillation, and the subsequent dynamics follows the incoherent motion of the slower component of timescale. In order to explore the origin of the quantum coherence in the short time region of Fig. 4(d), we consider the following minimal model:

$$H(\mathbf{q}) = |1\rangle\varepsilon_1(\mathbf{q})\langle 1| + |2\rangle\varepsilon_2(\mathbf{q})\langle 2| + |1\rangle J_{12}\langle 2| + |2\rangle J_{12}\langle 1|, \tag{3.3}$$

with

$$\varepsilon_1(\mathbf{q}) = \varepsilon_1^0 + \frac{\hbar\omega_\gamma}{2}(q_1 - d_\gamma)^2 + \frac{\hbar\omega_\gamma}{2}q_2^2, \tag{3.4a}$$

$$\varepsilon_2(\mathbf{q}) = \varepsilon_2^0 + \frac{\hbar\omega_\gamma}{2}(q_2 - d_\gamma)^2 + \frac{\hbar\omega_\gamma}{2}q_1^2, \tag{3.4b}$$

where the electronic excited state of the jth site is coupled to a single phonon mode, $\hbar\omega_\gamma q_j^2/2$, and the reorganization energy is expressed as $\lambda_\gamma=\hbar\omega_\gamma d_\gamma^2/2$. The Hamiltonian Eq. (3.3) can be easily diagonalized, and then we can obtain adiabatic potential surfaces,

$$E^\pm(\mathbf{q}) = \frac{\varepsilon_1(\mathbf{q}) + \varepsilon_1(\mathbf{q})}{2} \pm \sqrt{J_{12}^2 + \frac{\varepsilon_1(\mathbf{q}) + \varepsilon_1(\mathbf{q})}{2}}. \tag{3.5}$$

In Fig. 5, we draw the adiabatic potential surface for the lower energy, $E^-(\mathbf{q})$, as a function of two phonon coordinates, q_1 and q_2. The parameters in this model are chosen to be $\varepsilon_1^0=100$ cm^{-1}, $\varepsilon_2^0=0$ cm^{-1}, $J_{12}=100$ cm^{-1}, $\omega_\gamma=\gamma=53.08$ cm^{-1}, and $\lambda_\gamma=\lambda=500$ cm^{-1}($d_\gamma=4.34$), which correspond to those in Fig. 4. Since the reorganization energy λ_γ is large compared with the electronic coupling J_{12}, we can observe two local minima which represent the two states, $|1\rangle=|\varphi_{1e}\rangle|\varphi_{2g}\rangle$ and $|2\rangle=|\varphi_{2e}\rangle|\varphi_{1g}\rangle$. Incoherent hopping EET describes the transition between the local minima. Attention

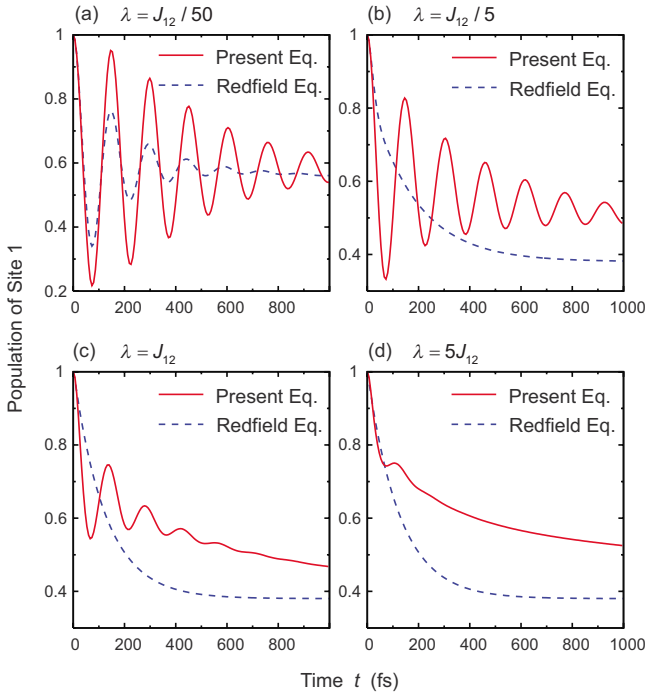

FIG. 6. (Color online) Time evolution of the population of site 1 calculated by the present theory, Eq. (2.23) (solid line) and the full-Redfield equation (dashed line) for various magnitudes of the reorganization energy λ. The other parameters are the same as those in Fig. 4, except $\gamma = 10.61\ \mathrm{cm}^{-1}(\gamma^{-1} = 500\ \mathrm{fs})$.

will now be given to the point of origin, which corresponds to the Franck–Condon state. The energy of the point is higher than the barrier between the minima; therefore, we find that the electronic excited state is delocalized just after the photoexcitation despite being in the incoherent hopping regime, $\lambda > J_{12}$. As time increases, the dissipation of reorganization energy proceeds and the excitation will fall off into one of the minima and become localized. It is interesting to note this phenomenon is equivalent of the localization or polaron formation, which has been studied extensively in literature of the solvated electron.[51] This picture is consistent with Fig. 4(d), where we observe quantum coherent motion on the timescale of the reorganization dynamics, $\gamma^{-1} = 100$ fs. The dynamic behavior of the intermediate regime, Fig. 4(c), can be understood as the combined influence of the slow fluctuation effect in the regime of small reorganization energy and the slow dissipation effect in the large reorganization energy as described in Fig. 5.

According to the above discussion, we can expect a longer lifetime of quantum coherent oscillation when the value of γ is smaller than that used in Fig. 4. Figure 6 gives the population dynamics of site 1 for the case of $\gamma = 10.61\ \mathrm{cm}^{-1}(\gamma^{-1} = 500\ \mathrm{fs})$. The other parameters are the same as in Fig. 4. In this slower fluctuation-dissipation case, the Markov approximation in the Redfield framework completely collapses. Figures 6(b)–6(d) reveal the longer-lasting coherent oscillation in comparison to Figs. 4(b)–4(d). In a case of small reorganization energy, the slower fluctuation sustains longer-lived coherent oscillation. In a case of large reorganization energy, on the other hand, the sluggish reorganization dynamics allow the excitation to stay above the barrier between two local minima of the adiabatic potential surface for a longer time in comparison to Fig. 4(d). Therefore, clear coherent oscillations emerge in Fig. 6(d) although the reorganization energy is large in comparison to the electronic coupling. In Fig. 6(a), however, the lifetime of oscillation is shorter than that in Fig. 4(a). This can be explained in terms of the inhomogeneity of the electronic energies, ε_1^0 and ε_2^0. Slow modulation of the electronic energies induced by the environmental phonons can be regarded as an inhomogeneous distribution of the energies. The destructive interference of various frequencies yields the shorter lifetime observed in Fig. 6(a). This is supported from the fact that the envelope of the oscillation is a Gaussian-like form, whose Fourier transform also shows a Gaussian-like form indicating inhomogeneous spectral broadening.

IV. CONCLUDING REMARKS

In this work, we have developed a new quantum dynamic equation for excitation energy transfer based on the Gaussian property of phonon operators, without employing the perturbative truncation. The equation can describe quantum coherent wavelike motion and incoherent hopping in the same framework. When timescale of reorganization is short compared to EET and reorganization energy is extremely small compared to any characteristic frequencies of EET (the Markov limit), the equation reduces to the conventional Redfield equation. On the other hand, when timescale of reorganization is short compared to EET and reorganization energy is large compared with intersite electronic coupling, the incoherent EET rate predicted by the equation is completely coincident with the Förster rate. In the regime of coherent wavelike motion, especially, the equation predicts several times longer lifetime of quantum coherence between electronic excited states of chromophores than the conventional Redfield equation does. Our approach shows that the quantum coherent motion can be observed even when reorganization energy is large in comparison to intersite electronic coupling. The reason of the long-lived quantum coherence is as follows: In a region of small reorganization energy, the slow fluctuation sustains longer-lived coherent oscillation, whereas the Markov approximation in the Redfield framework causes the infinitely fast fluctuation and then collapses the quantum coherence. In the region of large reorganization energy, on the other hand, the sluggish reorganization dynamics allows the excitation to stay above an energy barrier separating two local minima, which correspond to the two sites in the adiabatic potential surface, for a prolonged time.

The derivation of the present equation, Eq. (2.23), is based on a restricted spectral distribution function, i.e., the Drude–Lorentz spectral density or equivalently the overdamped Brownian oscillator model, Eq. (2.19). It is possible to extend the present framework to cases of arbitrary spectral distribution functions with help from the Meier–Tannor numerical decomposition scheme,[52]

$$\chi_j''[\omega] \simeq \sum_{\alpha=1}^{N} p_{j\alpha} \frac{\omega}{[(\omega+\Omega_{j\alpha})^2+\Gamma_{j\alpha}^2][(\omega-\Omega_{j\alpha})^2+\Gamma_{j\alpha}^2]}. \tag{4.1}$$

This decomposition allows us to express the symmetrized correlation function $S_j(t)$ and the response function $\chi_j(t)$ as sums of exponential functions, and then we can develop a theory for the spectral distribution function, Eq. (4.1), in similar fashion as described below Eq. (2.21). However, the mathematical expressions of the resultant equations of motion will be cumbersome and complicated, containing large quantities of parameters. Recently Jang *et al.*[14] developed another quantum dynamic equation to interpolate between the Redfield limit and the Förster limit by combining the small polaron transformation[10,53–56] and a second-order quantum master equation formalism. Their equation is applicable to arbitrary spectral distribution functions. It will be interesting to compare our reduced hierarchy approach with their small polaron approach. We consider this is a topic for future work.

In this paper we treated a dimer system in order to make discussion simple. Generalization of the present theory to multichromophoric systems is straightforward. Multichromophoric systems may also exhibit other origins of long-lived quantum coherence and its interplay of protein environment such as environment-induced coherence transfer processes.[57] The region of applicability of the full Redfield equation involves such small values of the reorganization energy that its application to photosynthetic systems seems highly problematic. In future work we will explore the application of the present approach to actual photosynthetic complexes.

ACKNOWLEDGMENTS

We thank Dr. Yuan-Chung Cheng for valuable comments. This work was supported by the Director, Office of Science, Office of Basic Energy Sciences, of the U.S. Department of Energy under Contract No. DE-AC02-05CH11231 and by the Chemical Sciences, Geosciences and Biosciences Division, Office of Basic Energy Sciences, U.S. Department of Energy under Contract No. DE-AC03-76SF000098. A.I. appreciates the support of the JSPS Postdoctoral Fellowship for Research Abroad.

[1] D. M. Jonas, Annu. Rev. Phys. Chem. **54**, 425 (2003).
[2] T. Brixner, T. Mancăl, I. V. Stiopkin, and G. R. Fleming, J. Chem. Phys. **121**, 4221 (2004).
[3] T. Brixner, J. Stenger, H. M. Vaswani, M. Cho, R. E. Blankenship, and G. R. Fleming, Nature (London) **434**, 625 (2005).
[4] G. S. Engel, T. R. Calhoun, E. L. Read, T.-K. Ahn, T. Mancăl, Y.-C. Cheng, R. E. Blankenship, and G. R. Fleming, Nature (London) **446**, 782 (2007).
[5] R. E. Fenna and B. W. Matthews, Nature (London) **258**, 573 (1975).
[6] Y.-F. Li, W. Zhou, R. E. Blankenship, and J. P. Allen, J. Mol. Biol. **271**, 456 (1997).
[7] S. I. E. Vulto, M. A. de Baat, S. Neerken, F. R. Nowak, H. van Amerongen, J. Amesz, and T. J. Aartsma, J. Phys. Chem. B **103**, 8153 (1999).
[8] H. van Amerongen, L. Valkunas, and R. van Grondelle, *Photosynthetic Excitons* (World Scientific, Singapore, 2000).
[9] H. Lee, Y.-C. Cheng, and G. R. Fleming, Science **316**, 1462 (2007).
[10] S. Rackovsky and R. Silbey, Mol. Phys. **25**, 61 (1973).
[11] R. Silbey, Annu. Rev. Phys. Chem. **27**, 203 (1976).
[12] S. Jang, M. D. Newton, and R. J. Silbey, Phys. Rev. Lett. **92**, 218301 (2004).
[13] Y.-C. Cheng and R. J. Silbey, Phys. Rev. Lett. **96**, 028103 (2006).
[14] S. Jang, Y.-C. Cheng, D. R. Reichman, and J. D. Eaves, J. Chem. Phys. **129**, 101104 (2008).
[15] A. G. Redfield, IBM J. Res. Dev. **1**, 19 (1957).
[16] A. G. Redfield, Adv. Magn. Reson. **1**, 1 (1965).
[17] W. T. Pollard, A. K. Felts, and R. A. Friesner, Adv. Chem. Phys. **93**, 77 (1996).
[18] V. May and O. Kühn, *Charge and Energy Transfer Dynamics in Molecular Systems*, 2nd ed. (Wiley-VCH, Berlin, 2004).
[19] S. I. E. Vulto, M. A. de Baat, R. J. W. Louwe, H. P. Permentier, T. Neef, M. Miller, H. van Amerongen, and T. J. Aartsma, J. Phys. Chem. B **102**, 9577 (1998).
[20] M. Cho, H. M. Vaswani, T. Brixner, J. Stenger, and G. R. Fleming, J. Phys. Chem. B **109**, 10542 (2005).
[21] A. Ishizaki and G. R. Fleming, J. Chem. Phys. **130**, 234110 (2009).
[22] S. Nakajima, Prog. Theor. Phys. **20**, 948 (1958).
[23] R. Zwanzig, J. Chem. Phys. **33**, 1338 (1960).
[24] F. Shibata, Y. Takahashi, and N. Hashitsume, J. Stat. Phys. **17**, 171 (1977).
[25] R. Kubo, Adv. Chem. Phys. **15**, 101 (1969).
[26] A. Ishizaki (unpublished).
[27] S. Mukamel, *Principles of Nonlinear Optical Spectroscopy* (Oxford University Press, New York, 1995).
[28] T. Takagahara, E. Hanamura, and R. Kubo, J. Phys. Soc. Jpn. **43**, 811 (1977).
[29] Y. Tanimura and R. Kubo, J. Phys. Soc. Jpn. **58**, 101 (1989).
[30] Y. Tanimura, J. Phys. Soc. Jpn. **75**, 082001 (2006).
[31] A. J. Leggett, S. Chakravarty, A. T. Dorsey, M. P. A. Fisher, A. Garg, and W. Zwerger, Rev. Mod. Phys. **59**, 1 (1987).
[32] M. Yang and G. R. Fleming, Chem. Phys. **275**, 355 (2002).
[33] H. Grabert, P. Schramm, and G.-L. Ingold, Phys. Rep. **168**, 115 (1988).
[34] T. M. Chang and J. L. Skinner, Physica A **193**, 483 (1993).
[35] D. Kohen and D. J. Tannor, J. Chem. Phys. **107**, 5141 (1997).
[36] D. Kohen, C. C. Marston, and D. J. Tannor, J. Chem. Phys. **107**, 5236 (1997).
[37] Y. C. Cheng and R. J. Silbey, J. Phys. Chem. B **109**, 21399 (2005).
[38] G. Katz, D. Gelman, M. A. Ratner, and R. Kosloff, J. Chem. Phys. **129**, 034108 (2008).
[39] J. Rammer, *Quantum Field Theory of Non-equilibrium States* (Cambrige University Press, New York, 2007).
[40] G. R. Fleming and M. Cho, Annu. Rev. Phys. Chem. **47**, 109 (1996).
[41] T. Förster, Ann. Phys. **437**, 55 (1948).
[42] T. Förster, in *Modern Quantum Chemistry Part III*, edited by O. Sinanoğlu (Academic, New York, 1965), pp. 93–137.
[43] R. Kubo, M. Toda, and N. Hashitsume, *Statistical Physics II: Nonequilibrium Statistical Mechanics*, 2nd ed. (Springer, Berlin, 1995).
[44] W. M. Zhang, T. Meier, V. Chernyak, and S. Mukamel, J. Chem. Phys. **108**, 7763 (1998).
[45] D. Zigmantas, E. L. Read, T. Mancăl, T. Brixner, A. T. Gardiner, R. J. Cogdell, and G. R. Fleming, Proc. Natl. Acad. Sci. U.S.A. **103**, 12672 (2006).
[46] K. Hyeon-Deuk, Y. Tanimura, and M. Cho, J. Chem. Phys. **127**, 075101 (2007).
[47] E. L. Read, G. S. Engel, T. R. Calhoun, T. Mancăl, T. K. Ahn, R. E. Blankenship, and G. R. Fleming, Proc. Natl. Acad. Sci. U.S.A. **104**, 14203 (2007).
[48] E. L. Read, G. S. Schlau-Cohen, G. S. Engel, J. Wen, R. E. Blankenship, and G. R. Fleming, Biophys. J. **95**, 847 (2008).
[49] A. Ishizaki and Y. Tanimura, J. Phys. Soc. Jpn. **74**, 3131 (2005).
[50] R. Zwanzig, *Nonequilibrium Statistical Mechanics* (Oxford University Press, New York, 2001).
[51] J. Zhao, B. Li, K. Onda, M. Feng, and H. Petek, Chem. Rev. (Washington, **106**, 4402 (2006).
[52] C. Meier and D. J. Tannor, J. Chem. Phys. **111**, 3365 (1999).
[53] I. I. Abram and R. Silbey, J. Chem. Phys. **63**, 2317 (1975).
[54] R. Silbey and R. A. Harris, J. Chem. Phys. **80**, 2615 (1984).
[55] R. A. Harris and R. Silbey, J. Chem. Phys. **83**, 1069 (1985).
[56] D. R. Reichman and R. J. Silbey, J. Chem. Phys. **104**, 1506 (1996).
[57] J. M. Jean and G. R. Fleming, J. Chem. Phys. **103**, 2092 (1995).